Automated Monitoring of Geolocation Consistency in Micro-satellite SAR Imagery

Angel Johnsy [1], Eyrin Kim[2], Qiaoping Zhang [1], Valentyn Tolpekin [1], Michael Wollersheim[1]

[1] ICEYE Oy, Maarintie 6, 02150 Espoo Uusimaa, Finland
(angel.johnsy,qiaoping.zhang,valentyn.tolpekin,michael.wollersheim)@iceye.com
[2] Stanford University, USA - eyrinkim@stanford.edu

Keywords: Geolocation accuracy, micro-SAR satellites, automated image-matching, offset detection

Abstract

High revisit-rate Synthetic Aperture Radar (SAR) constellations generate large volumes of imagery that require consistent geolocation accuracy to support applications such as change detection and interferometry. However, variations in orbit determination, attitude knowledge, and external factors such as Global Navigation Satellite System (GNSS) interference can introduce geolocation errors that vary across acquisitions, making large-scale validation challenging. This study presents an automated approach to detect and quantify geolocation offsets in ICEYE SAR imagery by aligning orthorectified scenes with reference images using feature-based matching and correlation-based refinement. The method is validated against independently derived absolute geolocation measurements from corner reflector calibration sites in the United States, Canada, Australia, and Poland. Evaluation across 726 acquisitions demonstrates strong agreement with reference measurements, achieving an overall root-mean-square error (RMSE) of 1.39 m, with RMSE values of 1.18 m for Spotlight mode and 1.93 m for Stripmap mode. Operational applicability is demonstrated through large-scale acquisition campaigns, including nationwide Stripmap coverage over Japan and coherent image stack analysis. The results show that the proposed method can reliably estimate geolocation offsets, detect anomalies, and monitor geometric consistency across large SAR archives, providing a practical and scalable solution for automated geolocation quality control in micro-satellite SAR constellations.

1. Introduction

High revisit-rate SAR constellations generate large volumes of imagery that must maintain consistent geolocation accuracy to support applications such as change detection, interferometry, and time-series analysis. While modern SAR systems can achieve meter-level absolute geolocation accuracy under nominal conditions, small deviations in orbit determination, attitude knowledge, or external factors such as Global Navigation Satellite System (GNSS) interference can introduce positional errors that vary across acquisitions. As constellation sizes and acquisition volumes grow, manual validation of geolocation accuracy becomes impractical, creating a need for automated, scalable methods to monitor geolocation consistency across large SAR archives.

Accurate SAR geolocation is critical for applications such as target identification, interferometry, and change detection, all of which depend on precise image co-registration. Large SAR missions such as TerraSAR-X, Sentinel-1, and COSMO-SkyMed have demonstrated centimeter- to meter-level geolocation accuracy through rigorous calibration and precise orbit determination (Balss et al., 2018; Schubert et al., 2015; Ager, 2009; ASI, 2019).

All SAR systems are affected by uncertainties in orbit determination, attitude knowledge, and auxiliary datasets such as digital elevation models (DEMs). In micro-satellite constellations, these effects can be more pronounced due to constraints on platform size, power, and onboard instrumentation, which can limit navigation and calibration performance. Moreover, GNSS-based orbit determination can be adversely affected by space-weather disturbances, such as geomagnetic storms (Zhao et al., 2024), as well as by intentional or unintentional GNSS interference, leading to increased positioning errors.

Traditional geolocation validation approaches rely on ground control points (GCPs), corner reflectors, or manual inspection. While corner reflector (CR) measurements provide highly accurate absolute geolocation validation, they are geographically sparse and only available at specific locations. As a result, most operational acquisitions cannot be directly validated using reflector-based methods. Furthermore, manual inspection becomes impractical at the constellation scale, where revisit frequency is high and data volumes are large.

ICEYE operates a large constellation of X-band SAR satellites with an active phased-array antenna enabling precise electronic beam steering. The product suite spans wide-area coverage modes (TOPSAR), providing scene extents of up to 200 × 500 km with spatial resolutions of approximately 15–27 m, as well as high-resolution Spotlight imagery covering 5 × 5 km to 15 × 15 km scenes with resolutions ranging from sub-meter down to approximately 0.2 m depending on acquisition mode and geometry. The ICEYE fleet includes several generations of satellites, with newer generations offering improved imaging capabilities, agility, and calibration performance (ICEYE, 2026).

To monitor and calibrate geometric integrity, images acquired over ground-surveyed calibration sites are used to compute root-mean-square error (RMSE) and evaluate horizontal geolocation accuracy. While this provides reliable absolute validation, it does not scale to global monitoring across all acquisitions.

To address this limitation, ICEYE’s “QuickOrtho” product, which provides reduced-resolution orthorectified imagery, enables rapid assessment of geolocation performance without requiring access to full-resolution data. By aligning test images with reference scenes and estimating relative offsets, it becomes possible to monitor geolocation consistency across large SAR archives.

In this study, we present an automated approach to detect and quantify geolocation offsets in ICEYE SAR imagery using feature-based image matching and correlation-based refinement. The proposed method is validated against independently derived corner reflector measurements and further evaluated in operational scenarios, including large-scale acquisition campaigns and coherent image stacks.

The main contributions of this work are:

(1) an automated and scalable framework for monitoring geolocation consistency across large SAR archives;

(2) a practical implementation leveraging reduced-resolution QuickOrtho products for efficient quality control;

(3) quantitative validation against independently derived corner reflector measurements across multiple global calibration sites;

(4) demonstration of operational applicability in large-scale acquisition campaigns and coherent stacks.

2. Methodology

2.1 Overview

Geolocation assessment quantifies how accurately a SAR pixel, mapped to geographic coordinates, corresponds to its true ground position. Absolute geolocation accuracy is the most common approach for geometric calibration and validation, typically measured using corner reflectors deployed at well-surveyed calibration sites. However, assessing geolocation performance at global scale across diverse landscapes requires an alternative approach. Relative geolocation accuracy can be estimated by aligning an orthorectified test SAR image with a reference SAR scene of known geometric quality.

Direct SAR-to-SAR image comparison is challenging, even for visual interpretation, due to geometric distortions inherent to side-looking radar imaging. For example, scenes acquired at shallow and steep incidence angles over the same area can exhibit significantly different geometric representations. As a result, careful reference image selection is critical for reliable alignment and offset estimation.

Reference images are selected based on similarity in acquisition geometry, including imaging mode, incidence angle, and look direction, to minimize geometric inconsistencies that could bias the offset estimation. When suitable reference data are available within the ICEYE archive, they are prioritized to maximize consistency. In cases where a close internal match is unavailable, orthorectified Sentinel-1 imagery (10 m resolution) is used as an external reference.

The analysis in this study employs ICEYE QuickOrtho products, which provide reduced-resolution orthorectified imagery optimized for rapid access, with pixel resolutions of approximately 12 m (Stripmap) and 2 m (Spotlight). Sentinel-1 data serve as a benchmark, offering absolute geolocation accuracies of approximately 2.5 m (Stripmap) and 7 m (Interferometric Wide) modes (Schubert et al., 2017; ESA, 2009). To ensure robustness under such variations in imaging geometry, the proposed approach relies on multi-scale feature detection and matching strategies designed to identify stable structures across differing resolutions and acquisition conditions.

2.2 Core Algorithm

Stable features are extracted from both the test and reference SAR images using a scale-space feature detector adapted for SAR imagery. The detector is designed to emphasize strong point scatterers and persistent structural features while suppressing speckle-induced artifacts. It operates by constructing a multi-scale pyramid representation of the image using Gaussian smoothing and identifying keypoints across different levels of the scale space (Lindeberg, 1998; Bay et al., 2008). Feature locations are selected based on the determinant of the Hessian, which highlights blob-like structures such as strong point scatterers and distinctive geometric features commonly observed in SAR imagery. This design allows the method to focus on stable scattering features that are more likely to remain consistent across varying imaging geometries.

The multi-scale representation enables the detection of corresponding features even when the images differ in spatial resolution. For example, an object may appear larger or smaller depending on image resolution, but can still be identified across different pyramid levels while preserving structural similarity. Local descriptors are computed around the detected keypoints using a scale-invariant feature transform (SIFT) framework to establish correspondences between the test and reference images (Lowe, 2004). Mismatched or unreliable correspondences are removed using a RANSAC-based outlier rejection procedure, ensuring that only geometrically consistent matches contribute to the offset estimation (Fischler and Bolles, 1981).

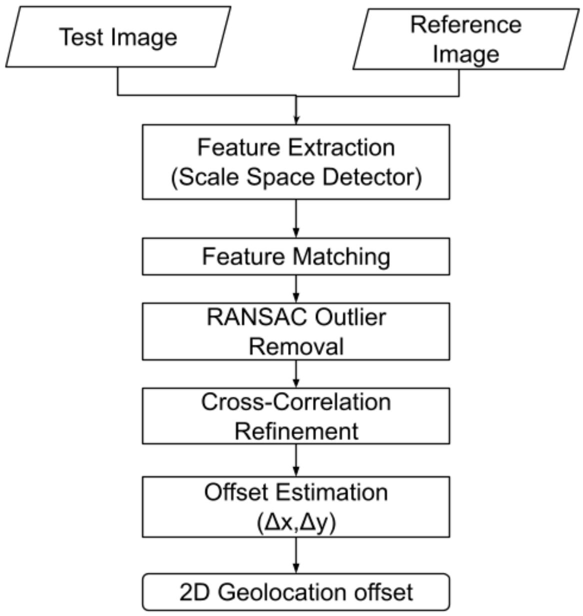

Figure 1. Flow Diagram of offset estimation between test and reference SAR image.

To further improve alignment accuracy, a correlation-based refinement is applied to the remaining matched features. Local cross-correlation is used to refine the displacement estimates

https://doi.org/10.5194/isprs-archives-XLIX-B3-2026-1359-2026

and compensate for residual mismatches. The statistically consistent offsets are then aggregated to compute the final displacement vector representing the relative geolocation difference between the test and reference scenes. Figure 1 illustrates the overall workflow of the offset estimation process.

3. Validation of the Methodology

The proposed algorithm is evaluated by comparing the estimated offsets with independently derived absolute geolocation measurements obtained from corner reflector calibration sites, which serve as ground-truth references.

Absolute geolocation accuracy is defined as the two-dimensional positional difference between the precisely surveyed geodetic coordinates of a corner reflector and the corresponding SAR image peak location, projected into the same terrestrial reference frame (Curlander and McDonough, 1991). The 2D offset error, computed from the ground-range and azimuth components, is defined as

$$2D\ Error = \sqrt{(\Delta x^2) + (\Delta y^2)} \qquad (1)$$

where Δx and Δy denote the offsets in the ground-range and along-track directions respectively. Figure 2 illustrates an example of geolocation offset estimation. The surveyed ground location of the corner reflector is shown in green, while the corresponding SAR image peak is indicated by a red cross. The displacement between these two positions defines the two-dimensional geolocation error.

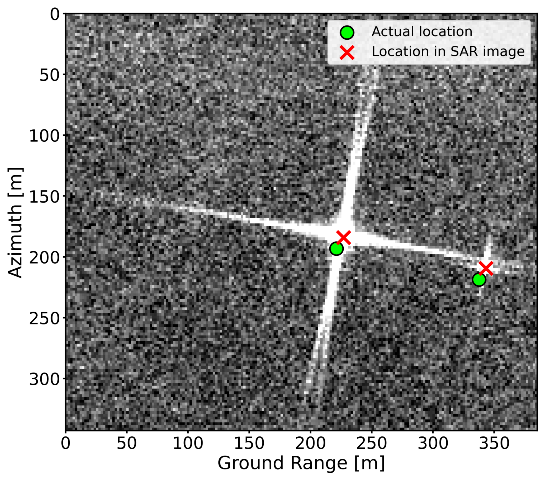

Figure 2. Example of geolocation offset estimation in SAR imagery. The green marker represents the surveyed ground location, while the red cross indicates the corresponding location measured in the SAR image.

3.1 Corner Reflector Calibration Sites

For absolute geolocation accuracy estimation, both public calibration sites and an ICEYE-operated calibration site were used. Absolute geolocation measurements from four geographically independent sites were used to validate the proposed relative geolocation estimation methodology.

Figure 3 illustrates the locations of the corner reflector sites used in this study, including Rosamond (USA), Okotoks (Canada), Surat Basin (Australia), and Wapno (Poland). These sites provide geographically diverse and independently validated reference measurements. The calibration sites are described below:

• Rosamond Corner Reflector Array (RCRA), California, USA
The Rosamond site consists of 38 corner reflectors representing multiple nominal sizes, with edge lengths of 0.7 m, 2.4 m, and 4.8 m. The site is widely used for SAR calibration and provides a stable, well-characterized reference environment (JPL, 2025).

• Okotoks, Canada (ICEYE calibration site)
The Okotoks site includes two large triangular corner reflectors, one oriented eastward and one westward. Each reflector has a side length of 1.7 m (Tolpekin et al., 2024).

• Surat Basin, Queensland, Australia
The Queensland calibration site consists of trihedral corner reflectors with edge lengths of 1.5 m, 2.0 m, and 2.5 m. The site is part of the CEOS Cal/Val infrastructure and provides an independent geographic validation environment (Thankappan et al., 2016).

• Wapno, Poland
The calibration site in Wapno contains 60 × 60 cm triangular corner reflectors that are precisely surveyed using high-precision GNSS measurements.

Figure 3. Corner reflector site locations.
Map tiles © Mapbox, © OpenStreetMap contributors

3.2 Dataset Description

A total of 726 acquisitions over the selected calibration sites were used for validation. The dataset spans a nine-month period from June 2025 to February 2026.

To ensure that the evaluation reflects the performance of the proposed methodology rather than errors introduced by poor reference scenes, only acquisitions with high-quality, independently validated reference images were included. Specifically, Spotlight reference images with absolute geolocation error below 1 m and Stripmap reference images with absolute geolocation error below 2 m were selected.

In addition to the absolute geolocation accuracy thresholds, the selected dataset spans multiple geographic regions and acquisition conditions, including variations in imaging geometry, incidence angle, and surface characteristics. This diversity ensures that the evaluation captures a representative range of operational scenarios and reduces the risk of bias toward specific scene types or calibration environments. Furthermore, the use of independently validated reference scenes minimizes the propagation of systematic errors into the relative offset estimation, enabling a more robust assessment of the proposed methodology.

The final dataset consists of 556 Spotlight and 170 Stripmap acquisitions. This distribution ensures representation across multiple calibration sites and acquisition modes. Table 1 summarizes the distribution of acquisitions by calibration site and acquisition mode.

Table 1. Number of acquisitions by calibration site and acquisition mode

Calibration Site	**Acquisition Mode**		**Count**
	Spotlight	**Stripmap**	
Okotoks,Canada	18	-	18
Queensland, Australia	-	73	73
Rosamond, USA	509	92	601
Wapno,Poland	29	5	34
Total	556	170	726

3.3 Quantitative Validation

The quantitative evaluation of the proposed methodology was performed by comparing the estimated offsets with independent reference measurements derived from corner reflector–based absolute geolocation accuracy. Error statistics were computed separately for Spotlight and Stripmap acquisition modes.

As summarized in Table 2, Spotlight mode achieves a root-mean-square error (RMSE) of 1.18 m with a mean error of 0.05 m, indicating negligible systematic bias. For Stripmap mode, the RMSE is 1.93 m, with a mean error of 0.77 m, reflecting slightly larger dispersion consistent with its coarser spatial resolution.

Table 2. Geolocation error statistics by acquisition mode

Acquisition Mode	**Mean Error**	**SD (m)**	**RMSE (m)**	**Samples (N)**
Spotlight	0.05	1.18	1.18	556
Stripmap	0.77	1.77	1.93	170
Overall	0.22	1.38	1.39	726

The near-zero mean error in Spotlight mode and low mean error in Stripmap acquisition mode confirm the absence of significant systematic bias in the proposed offset estimation approach. The overall RMSE of 1.39 m across 726 acquisitions demonstrates strong agreement between the algorithm-derived offsets and the independent corner reflector references. This level of accuracy indicates that the proposed method can reliably estimate geolocation offsets and has the potential to support improved geolocation performance when integrated into correction or calibration workflows.

It should be noted that the reference offsets are derived in the slant plane, whereas the ICEYE QuickOrtho products used in this study are orthorectified. Consequently, residual discrepancies may reflect a combination of projection differences, DEM-related inaccuracies, and differences between slant-range and map-projected geometries, in addition to algorithmic estimation errors.

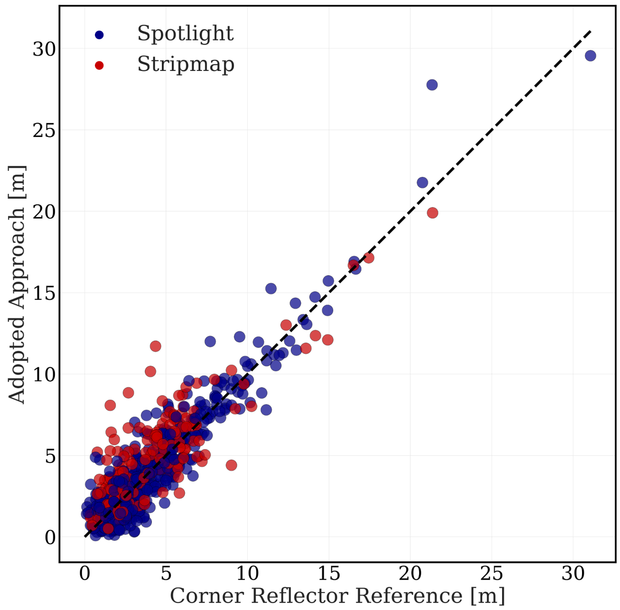

Figure 4. Comparison of geolocation offsets estimated using the proposed approach (y-axis) with independent corner reflector reference measurements (x-axis). The dashed diagonal line represents the 1:1 reference indicating perfect agreement.

Figure 4 illustrates the relationship between the geolocation offsets estimated using the proposed approach and the independent corner reflector (CR) reference measurements. The dashed line represents the 1:1 reference line indicating perfect agreement. Spotlight acquisitions are shown in blue, while Stripmap acquisitions are shown in red. The majority of the points are tightly clustered around the reference line, demonstrating strong consistency between the estimated offsets and the CR-derived reference values.

A slightly larger dispersion is observed for Stripmap acquisitions. This can be attributed to coarser spatial resolution of Stripmap QuickOrtho products, as well as the reference scene selection criteria, where Stripmap reference images with absolute geolocation errors of up to 2 m were included.

The distribution of points around the 1:1 reference line indicates that the method does not introduce systematic bias in the estimated offsets. The remaining spread reflects a combination of measurement noise, differences in imaging geometry, and residual uncertainty in the reference data. The consistent relationship across a range of offset magnitudes suggests the proposed approach remains stable for small and moderate geolocation errors, supporting operational monitoring.

The coefficient of determination (R^2), which quantifies the strength of the linear relationship between the estimated and reference offsets, further supports this agreement. When considering all acquisitions together, the overall R^2 value is 0.83, indicating strong correlation. When analyzed separately by acquisition mode, Spotlight imagery shows a higher correlation ($R^2 = 0.88$), while Stripmap imagery yields $R^2 = 0.70$, reflecting the increased variability associated with its coarser spatial resolution.

4. Operational Scale Validation

While the previous section validated the method using calibration targets, this section evaluates its performance under operational conditions using two representative use cases that reflect real-world acquisition scenarios. In the absence of calibrated targets, the results were additionally assessed through visual inspection of stable scene features.

For this purpose, clearly identifiable features were used as reference points. In urban environments, landmarks such as road intersections, building corners, and airport runways provide reliable tie points, while smaller structures such as light poles enable fine-scale validation in high-resolution Spotlight imagery. In natural terrain, features such as coastlines, river boundaries, and mountain ridges serve as stable references.

4.1 Monthly Japan Coverage Campaign

The first use case evaluates the algorithm on a monthly Stripmap acquisition campaign covering the entire territory of Japan. This dataset represents a typical operational scenario in which geolocation consistency must be monitored across a large number of acquisitions without the availability of ground calibration targets.

A total of 297 Stripmap acquisitions from the January 2026 campaign were analyzed, and geolocation offsets were estimated using the operational processing framework. The majority of scenes exhibit small geolocation offsets, with 74.4% showing offsets below 10 m and 19.5% within the 10–20 m range. Only 5.4% of scenes fall between 20 m and 100 m, while two acquisitions (0.7%) exceed 100 m, indicating potential geolocation anomalies.

These results demonstrate that the proposed approach can effectively monitor geolocation consistency at national scale and reliably identify outliers in large operational acquisition campaigns. Figure 5 illustrates the spatial coverage of Japan, with colors representing the magnitude of the estimated geolocation offsets.

4.2 Coherent Stack Monitoring

The second use case demonstrates the application of the proposed method for monitoring geolocation consistency over coherent acquisition stacks. Maintaining stable geolocation across repeated acquisitions with identical imaging geometry is critical for applications such as Interferometric SAR (InSAR), change detection, and Persistent Scatterer Interferometry (PSI).

The temporal behavior of the estimated offsets provides additional insight into the stability of the geolocation performance across repeated acquisitions. In coherent stacks with identical imaging geometry, variations in estimated offsets are expected to reflect underlying geolocation inconsistencies rather than differences in acquisition configuration. As such, the observed stability over time suggests that the proposed method is capable of consistently capturing relative geolocation variations under controlled acquisition conditions.

From an operational perspective, this capability enables continuous monitoring of geolocation consistency within coherent acquisition campaigns. Deviations from the expected temporal stability can be used as indicators of potential anomalies, such as orbit determination errors or calibration issues, allowing for early detection and investigation without requiring dedicated calibration targets.

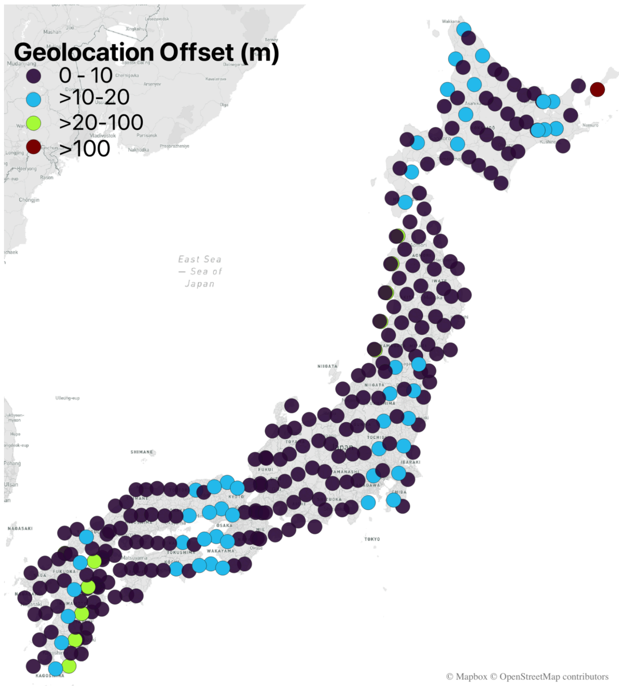

Figure 5. January 2026 Stripmap acquisition coverage over Japan with colors representing the geolocation errors. Map tiles © Mapbox, © OpenStreetMap contributors

Figure 6 presents the estimated geolocation offsets for a coherent stack of 24 Spotlight acquisitions collected over São Paulo, Brazil, spanning 25 days from 30 January 2026 to 23 February 2026, with identical imaging geometry. The estimated offsets remain stable over time, with most values within a few meters. Across the 24 acquisitions, the mean geolocation offset is 1.98 m, with a median of 1.8 m and a standard deviation of 1.07 m, and the observed offsets range from 0.38 m to 4.10 m.

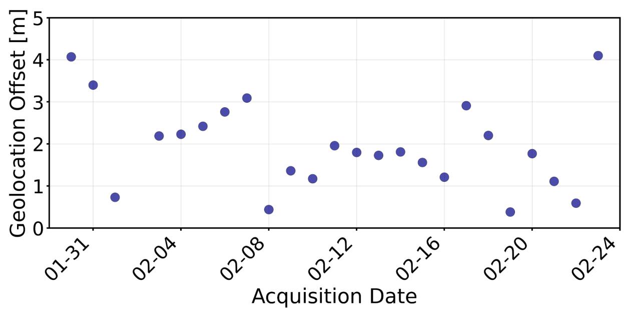

Figure 6. Acquisition date versus geolocation offset [m]

In this analysis, all offsets are computed relative to a reference image with independently validated geolocation accuracy, allowing the estimated offsets to reflect relative variations within the stack. In an operational context, this enables identification of acquisitions that deviate from the expected offset range, providing a mechanism to flag and mitigate potential outliers prior to interferometric processing, where even small inconsistencies can impact co-registration quality or introduce phase ramps.

This level of temporal consistency indicates that the proposed approach produces stable offset estimates across repeated acquisitions, supporting its use as a monitoring tool for geolocation consistency within coherent acquisition stacks. It should be noted that this analysis does not provide independent validation of absolute accuracy, but rather demonstrates the internal consistency of the estimated offsets.

The São Paulo stack represents a dense urban environment where SAR geometric distortions such as layover are prominent due to tall buildings and closely spaced structures. In such conditions, light poles act as strong point scatterers and provide reliable reference points for visual inspection. Figure 7(a) shows the QuickOrtho SAR image with detected point targets corresponding to several light poles, while Figure 7(b) presents the corresponding optical image with the true locations of these light poles marked in red. The close spatial agreement between the SAR-derived positions and the optical reference supports the reliability of the estimated geolocation offsets.

(a) (b)

Figure 7. SAR image (a) and optical image(b) with light poles location highlighted in red circle. Optical image © Google

5. Conclusion

This study introduced an automated framework for monitoring geolocation consistency in ICEYE SAR imagery using feature-based image alignment combined with correlation-based refinement. Validation against independently derived corner reflector measurements demonstrated strong agreement between the estimated offsets and reference data, achieving an overall RMSE of 1.39 m across 726 acquisitions. The results indicate that the proposed method can reliably estimate relative geolocation offsets with minimal systematic bias across both Spotlight and Stripmap acquisition modes.

Beyond calibration-site validation, the approach was demonstrated in operational scenarios, including nationwide acquisition campaigns and coherent stack monitoring. These use cases highlight the capability of the method to detect geolocation anomalies and track temporal stability across large SAR acquisition archives. Such automated monitoring is particularly valuable for micro-satellite SAR constellations, where high revisit rates and data volumes make manual inspection impractical.

Future work will focus on extending the analysis to larger datasets and more diverse imaging conditions to better characterize sources of geolocation variability across regions, acquisition times, and satellite platforms. In addition, future research will explore the integration of deep learning based feature detection and matching approaches to improve robustness under varying imaging geometries, including differences in incidence angle, look direction, and acquisition configuration.

Overall, the proposed framework provides a practical and scalable solution for continuous, automated monitoring of geolocation consistency across large micro-satellite SAR constellations.

References

Ager, T., 2009. Geometric precision in space radar imaging: Results from TerraSAR-X. *Proceedings of the ASPRS Annual Conference*, Baltimore, Maryland, USA, March 9–13, 2009.

ASI, 2019. *COSMO-SkyMed Mission and Products Description*, Rev. 3.1. Agenzia Spaziale Italiana (ASI), Rome, Italy.

Balss, U., Gisinger, C. and Eineder, M., 2018. Measurements on the absolute 2-D and 3-D localization accuracy of TerraSAR-X. *Remote Sensing*, 10(4), 656. https://doi.org/10.3390/rs10040656

Bay, H., Ess, A., Tuytelaars, T., Van Gool, L., 2008. Speeded-Up Robust Features (SURF). *Computer Vision and Image Understanding*, 110(3), 346–359.

Curlander, J. C., and McDonough, R. N., 1991. *Synthetic Aperture Radar: Systems and Signal Processing*. Wiley, New York.

ESA, 2009. *Sentinel-1 Product Definition* (Issue date 24 June 2009). European Space Agency.

Fischler, M.A., Bolles, R.C., 1981. Random sample consensus: A paradigm for model fitting with applications to image analysis and automated cartography. *Communications of the ACM*, 24(6), 381–395.

ICEYE, 2026. ICEYE SAR Product Documentation: Latest Releases. Available at: https://sar.iceye.com/latest (last access: 27 Mar 2026).

JPL, 2025. Rosamond Calibration Array. Available at: https://uavsar.jpl.nasa.gov/cgi-bin/calibration.pl (last access: 6 Nov 2025).

Lindeberg, T., 1998. Feature detection with automatic scale selection. International Journal of Computer Vision, 30(2), 79–116.

Lowe, D.G., 2004. Distinctive image features from scale-invariant keypoints. *International Journal of Computer Vision*, 60(2), 91–110.

Schubert, A., Miranda, N., Geudtner, D. and Small, D., 2015. Sentinel-1A product geolocation accuracy: commissioning phase results. *Remote Sensing*, 7(7), 9431–9449. https://doi.org/10.3390/rs70709431

Schubert, A., Hajnsek, I., Gisinger, C., Krieger, G., Werninghaus, R. and Wegmüller, U., 2017. Sentinel-1A/B combined product geolocation accuracy. *Remote Sensing*, 9(6), 607. https://doi.org/10.3390/rs9060607

Thankappan, M., Balss, U., Garthwaite, M., Gisinger, C., Meadows, P., Boncori, J. P. M., and Schubert, A., 2016. Calibration of Sentinel-1 and TerraSAR-X time-series SAR data over the Queensland corner reflector array, Australia. CEOS WGCV SAR Calibration and Validation Workshop.

Tolpekin, V., Wollersheim, M., Zhang, Q., and Kulshrestha, A., 2024. SAR interferometry using new space SAR constellation: application and validation. In: *Proceedings of the AGU Fall Meeting 2024*, Abstract G33C-07.

Zhao, D., Cui, S., Zhang, X., Li, L., Sun, P., Bian, C., Ban, W., Hancock, C.M., Wang, Q. and Zhang, K., 2024. Analysis of global ionospheric scintillation and GPS positioning interference triggered by full-halo CME-driven geomagnetic storm: A case study. *Advances in Space Research*, 74(5), 2492–2509. https://doi.org/10.1016/j.asr.2024.06.001

https://doi.org/10.5194/isprs-archives-XLIX-B3-2026-1359-2026